Preparation, Characterization and Structure Trends for Graphite Intercalation Compounds Containing Pyrrolidinium Cations

Hanyang Zhang,[†] Yuanyuan Wu,[†] Weekit Sirisaksoontorn,[‡] Vincent T. Remcho[†] and Michael M. Lerner*,[†]

[†]Department of Chemistry, Oregon State University, Corvallis, Oregon 97331-4003, United States

[‡]Department of Chemistry and Centre of Excellence for Innovation in Chemistry, Faculty of Science, Kasetsart University, Chatuchak, Bangkok 10900, Thailand

ABSTRACT: New graphite intercalation compounds (GICs) containing *N, N*-n-alkyl substituted pyrrolidinium cation intercalates ($Py_{n.m}$, n, m= alkyl chain lengths) are obtained via cationic exchange from stage-1 donor-type GIC $[Na(ethylenediamine)_{1.0}]C_{15}$. Powder X-ray diffraction and thermogravimetric analyses are used to determine the GIC structures and compositions. $[Py_{4.8}]C_{47}$·0.71DMSO and $[Py_{8.8}]C_{48}$ with intercalate monolayers are obtained as stage-1 GICs with gallery expansions of 0.48 nm, whereas $[Py_{1.18}]C_{47}$ and $[Py_{12.12}]C_{80}$·0.25DMSO form stage-1 GICs with intercalate bilayers and gallery expansions of 0.81 nm. The gallery dimensions require that alkyl-chain substituents orient parallel to the encasing graphene sheets. Smaller intercalate cations such as $Py_{1.4}$, $Py_{4.4}$, and $Py_{1.8}$ either form high-stage GICs, or do not form stable intercalation compounds. These results, along with those reported for graphite intercalation of other quaternary ammonium cations, indicate trends in graphite chemistry where larger intercalates form more stable and lower-stage GICs, and the graphene sheet charge densities can be correlated to the intercalate footprint areas.

■ INTRODUCTION

Graphite is a prototypical and also technologically-important intercalation host and graphite intercalation compounds (GICs) have long been studied for their interesting and useful structures and properties. [1-4] Either cations or anions, sometimes accompanied by neutral co-intercalates, can be introduced between the graphene layers via chemical or electrochemical redox reactions to form variety of GICs. The accompanying reduction or oxidation of the graphene sheets results in so-called donor-type or acceptor-type GICs, respectively. [5-10] Graphite is unique in forming highly-ordered stages, i.e. ordered sequences of graphene sheets and intercalate galleries, where the stage number is the sequence descriptor. [11] In a stage-1 GIC, each graphene sheet is separated from the others by intercalate galleries, whereas a stage-2 GIC has two adjacent graphene sheets contained between intercalate galleries, and *etc*. The gallery expansion, Δd, describes the distance along the direction perpendicular to the host sheet, that separates the graphene sheets encasing each intercalate gallery. [12]

GICs have several important applications today, including the use of lithiated graphite, LiC_x, as a battery anode, [13-15] and in the production of exfoliated graphites that serve as gas or heavy oil absorbents [16-18] or in the manufacture of thermally-stable seals. [19] Graphite sulfate is the common GIC used to make exfoliated graphite, although many other GICs have been reported or proposed for this purpose, [20-23] including those containing quaternary ammonium cations. [24, 25]

Quaternary ammonium cations, including symmetric or asymmetric tetra-n-alkylammonium (TAA) and pyrrolidinium ($Py_{n.m}$, where n and m indicate alkyl chain lengths), are reductively stable [26-28] and are therefore good candidates for GIC chemistry. We previously reported the preparation of a homologous series of TAA-GICs by either cation exchange of TAA^+ for $Na(en)^+$ in stage-1 $[Na(en)_{1.0}]C_{15}$ (en=ethylenediamine), [29] or by the electrochemical reduction of graphite in a TAABr/DMSO electrolyte. [30] The ionic radii of TAA cations in solution increase regularly with increasing alkyl chain length, for example, compare $(C_4H_9)_4N^+$ (T4A) r~0.4 nm to $(C_8H_{17})_4N^+$ (T8A) r~1.4 nm. However, the gallery expansions in the corresponding TAA-GICs do not show a similar dependence on cation size. The Δd values are either ~0.4-0.5 nm (for monolayers) or ~0.8 nm (bilayers). Electrochemical studies indicate that TAA-GICs with smaller TAA cations can form *in situ* but are not sufficiently stable to be isolated [5, 31, 32] without a surface passivation step. [33]

Several studies describe the intercalation of quaternary ammonium cations into graphite during electrochemical reduction in organic solvents and ionic liquids. Katayama *et al*. [34] reported $Py_{1.4}$ intercalation into graphite electrodes during reduction of the ionic liquid electrolyte LiTFSI / *N*-butyl-*N*-methylpyrrolidinium bis(trifluoromethylsulfonyl)

imide ($Py_{1.4}TFSI$). Ethylene carbonate was added to form a passivation layer that slowed organic cation intercalation. Zheng *et al*. [35] used cyclic voltammetry to identify reversible intercalation/deintercalation of $(CH_3)_3(C_6H_{13})N^+$ cations into graphite anodes in an ionic liquid electrolyte.

We report below the preparation of a homologous series of *N,N*-pyrrolidinium GICs (Py-GICs) using a cation exchange method, characterization of the product structures and compositions, and discuss the broader relation of intercalate structure to GIC stability and composition.

■ EXPERIMENTAL

Materials and syntheses. Graphite powder (SP-1 grade with average diameter 100 μm, Union Carbide), sodium metal (99.9%, Sigma-Aldrich), and 1-butyl-1-methylpyrrolidinium bromide (>97.0%, Tokyo Chem. Ind.) were used as received. Ethylenediamine (en, 99%), dimethylsulfoxide (DMSO, 99.9% AR grade), acetonitrile (MeCN, 99.9% HPLC grade) and methanol (MeOH, 99.9%) were all dried over 4Å molecular sieve prior to use. All chemicals except for MeOH were stored in an N_2-filled glovebox.

All Py cations employed were synthesized as bromide salts by according to literature methods, [36, 37] and their structures confirmed using ^{1}H-1D nuclear magnetic resonance (NMR). (See SI, section 1) The $[Na(en)_{1.0}]C_{15}$ precursor for ion exchange was prepared according to a previously published method. [38, 39]

For all Py cations except for $Py_{12.12}$ and $Py_{1.18}$, the bromide salts (0.20 mmol) and $[Na(en)_{1.0}]C_{15}$ (0.30 mmol) were placed in a glass tube, then 2.0 mL of DMSO was added and the tube sealed under N_2. To prevent gel formation with the less soluble $Py_{12.12}$ and $Py_{1.18}$ salts, they were dissolved into DMSO (2.0 mL) and stirred for 24 h prior to addition of the GIC. In the sealed tubes, the reactants were rapidly heated to 80°C and stirred for 10 min, then centrifuged (3,200 rpm, 2 min) to isolate the solid product and to collect the supernatant for future analysis. The wet Py-GIC products were rinsed briefly with MeCN, then with anhydrous MeOH, and then dried *in vacuo* at 60°C for 72 h. A reaction scheme is provided in Scheme 1.

Characterization. Powder X-ray diffraction (PXRD) patterns were acquired using a Rigaku Miniflex II diffractometer with Ni-filtered CuKα radiation (λ= 0.15406 nm). All measurements were collected in the 2θ range from 3 to 60° at a scan rate of 3°/min. The following equation was applied to describe the relationship between the observed periodic distance along c-axis (I_c), the gallery expansion (Δd), and the GIC stage (n):

$$I_c = \Delta d + n \times 0.335 \text{ nm} \quad (1)$$

where 0.335 nm is the thickness of a single graphene sheet. To evaluate the extent of the cation exchange of Py cations for $Na(en)^+$, the supernatant collected from each reaction was evaluated using capillary zone electrophoresis (CZE). CZE employed a Hewlett-Packard ^{3}DCE station and a method adopted from a literature reference. [39] Further details are provided in SI Section 2. A TA Q50 thermogravimetric analyzer (TGA) was used to evaluate mass loss from ambient to 800 °C at 10 °C/min under N_2 flow (60 mL/min). Energy-minimized structural models for Py cation conformations were calculated using the hybrid density functional method (B3LYP) with a 6-31G* basis set on Gaussian 09W software. One-dimensional electron density maps were generated from structure models and experimental PXRD data using a method reported previously. [40]

■ RESULTS AND DISCUSSION

Structural characterization of products. The PXRD patterns for all obtained products and the graphite and $[Na(en)_{1.0}]C_{15}$ precursors are shown in Figure 1. $[Na(en)_{1.0}]C_{15}$ (Figure 1b) is obtained as a stage-1 phase with Δd=0.36 nm, corresponding to the monolayer arrangement of cationic complex $[Na(en)]^+$ in intercalate galleries, with the co-intercalate en chelating the alkali metal cations and oriented nearly parallel to the graphene sheets. [38] Figure 1e and f show stage 1 products $[Py_{8.8}]C_x$ and $[Py_{4.8}]C_x$, with Δd=0.49 and 0.48 nm, respectively, whereas Figure 1c and d indicate single-phase stage 1 Py-GICs with Δd=0.81 nm. Electron density maps derived from the PXRD peak intensity data (see Figure 3) further support the presence of intercalate monolayers and bilayers, respectively, for smaller and larger gallery expansions. Compositional data (see below) help confirm these assignments. For all these GICS, the Py cations must be highly flattened relative to the solution phase conformations to fit within the observed gallery dimensions, as

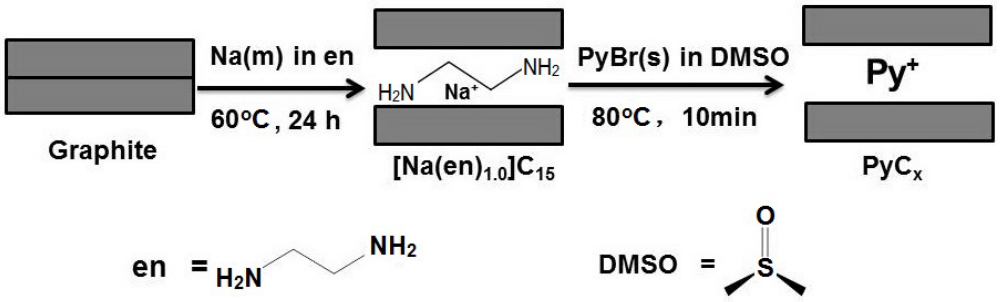

Scheme 1. Synthetic scheme for Py-GIC syntheses

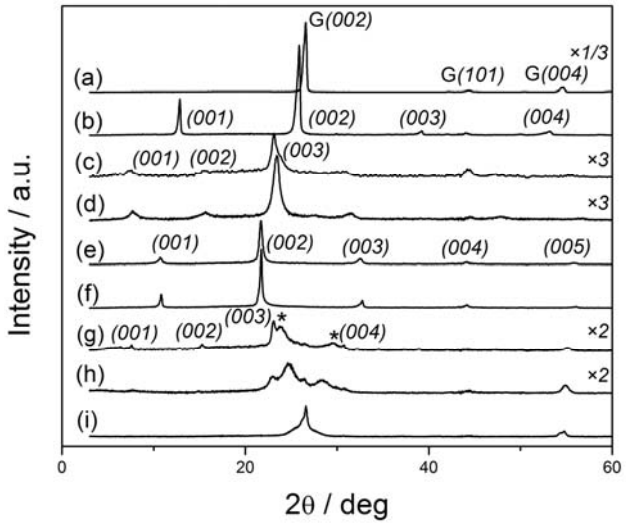

Figure 1. PXRD patterns for (a) graphite, (b) $[Na(en)_{1.0}]C_{15}$, and for GICs formed by exchange with the following cations; (c) $Py_{12.12}$, (d) $Py_{1.18}$, (e) $Py_{8.8}$, (f) $Py_{4.8}$, (g) $Py_{1.8}$, (h) $Py_{4.4}$, and (i) $Py_{1.4}$. In (g), the stage 3 product peaks are marked *.

has been observed previously with large TAA cations in GICs.[29, 30]

Exchange with $Py_{1.8}$ (Figure 1g) shows a mixed phase with stages 2 and 3 GIC product, along with graphite, and the derived Δd=0.49 nm indicating again a monolayer intercalate gallery in the GICs. Compositional analyses (below) confirm the low intercalate content following this reaction. Exchange with $Py_{4.4}$ (Figure 1h) produces a high-stage GIC ($n \geq 6$). A cation exchange reaction with $Py_{1.4}$ results in a disordered product displaying only broadened graphite diffraction peaks (Figure 1i).

In sum, new single-phase, stage-1 GICs are obtained by cation exchange of the $Na(en)^+$ complex intercalate for the larger Py cations, whereas these reactions using smaller Py cations result in high-stage and/or a disordered graphitic product. All the low-stage GIC products are flat black, in contrast to the bright blue $[Na(en)_{1.0}]C_{15}$ precursor.

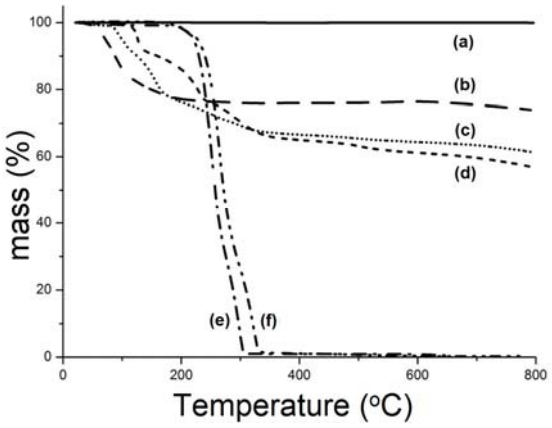

Figure 2. TGA mass loss data for (a) graphite, (b) $[Na(en)_{1.0}]C_{15}$, (c) $Py_{4.8}$GIC, (d) $Py_{1.18}$GIC, (e) $Py_{4.8}$Br, and (f) $Py_{1.18}$Br.

Capillary zone electrophoretic analyses. Capillary zone electrophoretic (CZE) analyses were used to follow the solution-phase concentration changes during the exchange reaction with $Py_{4.8}$. The Py cation concentration was monitored along with Na^+ and en, which appear in the superna tant during the cation exchange. The analysis results were applied to Equation 2:

$$[Na(en)_{1.0}]C_{15} + Py_{4.8}^+ \rightarrow [Py_{4.8}]C_{44} + a\,Na+ + b\,en \quad (2)$$

Calculated values for stoichiometric coefficients a and b were 1.05(7) and 1.01(6), respectively, confirming near quantitative displacement of the sodium complex intercalate (see also SI, section 2). The value x=44(3) in the product is obtained from the $Py_{4.8}$ loss from the reactant solution and agrees with that obtained from TGA (x=47, see below).

Thermoanalysis. The TGA mass loss plots for representative products are displayed in Figure 2. The Py-GIC products obtained (Figure 2c and d) exhibit multiple step mass losses. The 27.6% and 37.5% mass losses between 110-550°C are associated with degradation of the Py cation intercalates. The corresponding pyrrolidinium bromide salts (Figure 2e and f) are stable to ≈200°C, demonstrating the often observed catalytic effect of intercalation on the thermolysis of

Table 1. Structural and compositional data, and derived packing fractions, of GIC products and the $[Na(en)_{1.0}]C_{15}$ precursor.

Intercalate cation	GIC stage	Δd / nm	Intercalate arrangement	Intercalate mass pct	Composition	Packing fraction
$Na(en)^+$	1	0.36	monolayer	30.4	$[Na(en)_{1.0}]C_{15}$	0.51
$Py_{1.4}$	n/a	n/a	n/a	5.3	n/a	n/a
$Py_{4.4}$	6+	0.52	monolayer	10.3	n/a	n/a
$Py_{1.8}$	2+	0.49	monolayer	7.0	n/a	n/a
$Py_{4.8}$	1	0.48	monolayer	34.5	$[Py_{4.8}]C_{47}$·0.71DMSO	0.57
$Py_{8.8}$	1	0.48	monolayer	33.5	$[Py_{8.8}]C_{48}$	0.59
$Py_{1.18}$	1	0.81	bilayer	38.1	$[Py_{1.18}]C_{47}$	0.41
$Py_{12.12}$	1	0.81	bilayer	29.7	$[Py_{12.12}]C_{80}$·0.25DMSO	0.30

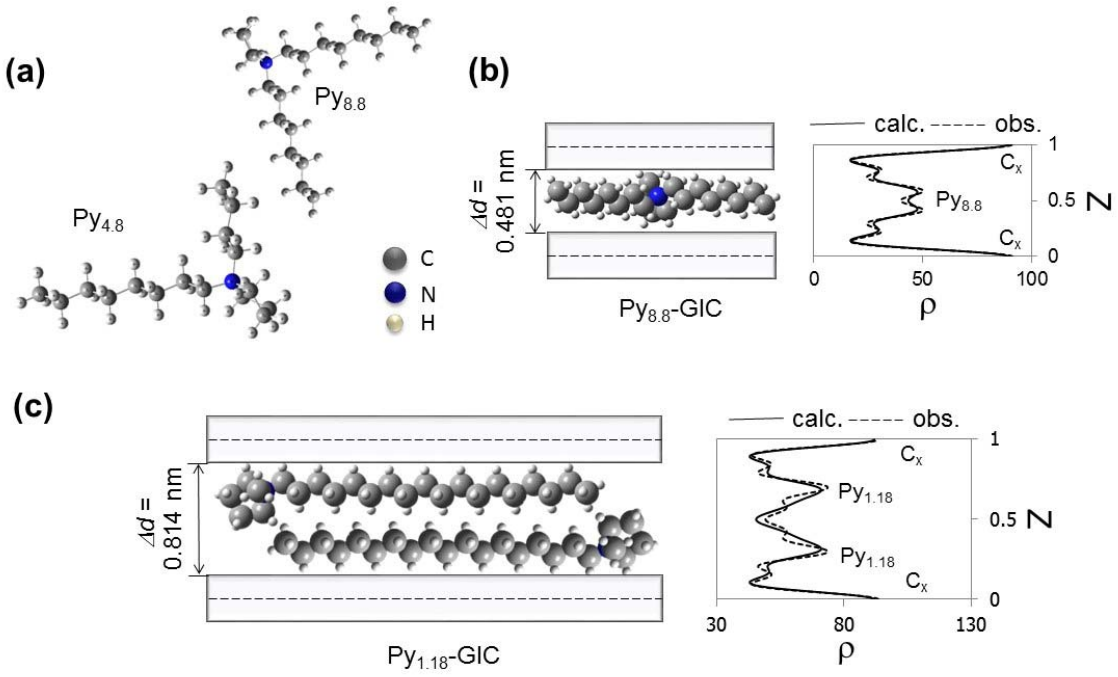

Figure 3. (a) Energy-minimized structure models for $Py_{4.8}$, $Py_{8.8}$ cations; structure models and experimental and calculated electron density maps for (b) monolayer $Py_{8.8}$-GIC and (c) bilayer $Py_{1.18}$-GIC.

the intercalates.[30] For $Py_{4.8}$GIC, the 5.1% of mass loss from 90-110°C can be ascribed to volatilization of DMSO co-intercalate, which has been previously demonstrated using TGA-MS analyses.[29] Mass losses above 550°C indicate further decomposition of the carbonaceous thermolysis products.[29, 30, 33, 39] Structural data and compositional data thus derived for the reactant products are summarized in Table 1.

Packing fraction. The gallery packing fractions for the GIC products are obtained by combining the structural and compositional data, according to Equation 3:

$$\text{packing fraction} = V_i / V_h \quad (3)$$

where V_i is the total van der Waals intercalate volume,[41] and V_h is the available volume in the expanded lattice. V_h can be calculated from the host surface area (0.0261 nm² / graphitic C), the expansion Δd along the stacking direction, and the GIC stage.[42] The derived packing fractions (Table 1) are significantly lower for the bilayer galleries than those containing monolayers.

Intercalate conformation calculations. Three low energy conformers have been proposed for isolated Py cations – *ax*-envelope, *eq*-envelope, and twist. When the alkyl chains remain in the *trans* conformation, the torsion energies are small and there is a correspondingly low transformation energy between the conformations (e.g. from $Py_{1.4}$ the energy barrier was reported as <5 kJ/mol).[43] When both alkyl chains are parallel to the encasing graphene sheets, all of three conformations have similar steric requirements that can be accommodated in the observed gallery expansions. (Figure 3) The low barriers and similar dimensional requirements preclude further distinctions on specific conformers present in the GIC products.

Structural trends for quaternary ammonium cation GICs. The preparation of TAA-GICs[29] and Py-GICs opens a rich area of investigation due to the abundance and range of possible substituent groups. The results obtained in both cases thus far show unanticipated trends – smaller cations do not form stable GICs without pre-passivating reactions,[33] whereas the extent of intercalate content increases generally with cation volume from higher stage to stage 1 monolayer to stage 1 bilayer. Figure 4 shows the relation of intercalate molar volume with product stage; from this summary we can state with somewhat more precision that stable GICs form with intercalates >0.2 nm³, stable stage 1 requires intercalates >0.2-0.3 nm³, and stage 1 bilayers are seen exclusively with intercalate volumes >0.4 nm³.

Since the values of "*x*" in $Cat^{+}C_x^{-}$ define the stoichiometric ratio of graphitic carbon atoms to sheet negative charge for a given stage, they are inversely proportional to the graphene sheet charge density (SCD). From the compositions derived for the Py-GIC products obtained, SCD decreases in all exchange reactions when compared to the starting GIC, $[Na(en)_{1.0}]C_{15}$, indicating that these exchange reactions also involve partial oxidation of the graphene sheets. The large *x*

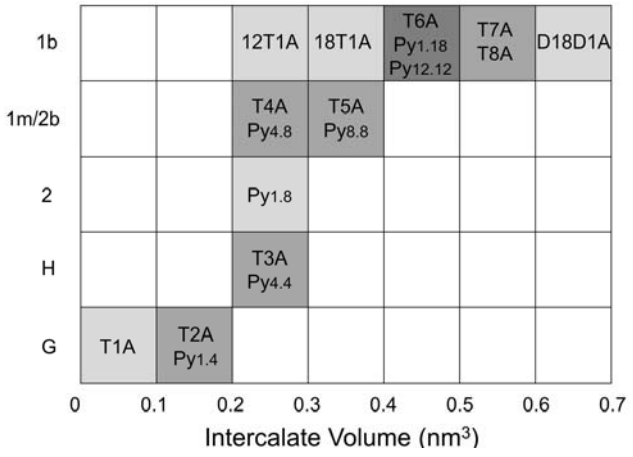

Figure 4. Structure map over intercalate volumes for quaternary ammonium-GICs. 12T1A= $(C_{12}H_{25})(CH_3)_3N^+$, 18T1A=$(C_{18}H_{37})(CH_3)_3N^+$, D18D1A= $(C_{18}H_{37})_2$ $(CH_3)_2$ N^+. X-axis labels: G=graphitic, H=high stage, 2=stage 2, 1=stage 1, m=monolayer and b=bilayer. Darker gray indicates more known examples.

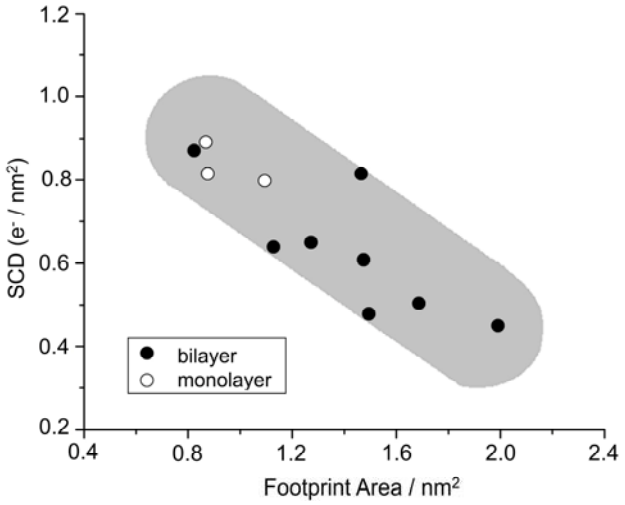

Figure 5. Graphene sheet charge densities (SCD) vs. intercalate footprint areas for stage 1 Py-GICs.

values (x=47-80) obtained for stage 1 products indicate that these large cation Py-GICs have unusually low SCDs. For example, donor-type GICs with smaller ions have stoichiometries such as C_6Li or C_8K.

One explanation for the low SCDs in these GICs lies in the steric interactions between large intercalates, this can also help explain the conversion from monolayer to bilayer arrangement with larger molar volume intercalates. If so, the steric dimensional requirements above (and below) each graphene sheet should correlate with the observed SCD. This correlation is markedly not present for most known GICs (for example, C_8M is obtained for stage 1 with M = K, Rb or Cs and "$C_{20\text{-}24}^+$" is the common stage 1 composition for a very broad range of anion intercalates).[7, 44-46] To explore this possibility, Py and TAA cation footprints were calculated from structure models (see SI, section 3) and plotted against the derived SCDs (Figure 5). Although the relation shows a range rather than a single linear fit, and very likely depends on other factors such as intercalate shape and packing, a strong correlation (γ= -0.85) exists where larger intercalates result in a lower SCD in the obtained GICs. This provides the first strong evidence for an energetic model where intercalate steric interactions play a role in the product composition and extent of graphene sheet reduction.

■ CONCLUSION

A novel series of Py-GICs were synthesized via cationic exchange method from stage-1 $[Na(en)_{1.0}]C_{15}$ precursor, with both structure and composition characterized. Among the new products obtained, $[Py_{4.8}]C_{47}$·0.71DMSO and $[Py_{8.8}]C_{48}$ were the stage-1 monolayer GICs, while the $[Py_{1.18}]C_{47}$ and $[Py_{12.12}]C_{80}$·0.25DMSO were stage-1 bilayer GICs. The molar intercalate volume required to obtain different GIC stages and orientations are described, and a clear relation is observed between intercalate footprint dimension and the graphene SCD, indicating that intercalate steric interactions play an important role in these reactions and product stabilities.

■ ASSOCIATED CONTENT

Supporting Information

Syntheses of pyrrolidinium bromide salts; capillary zone electrophoresis and footprint area calculation. This material is available free of charge via the Internet at http://pubs.acs.org.

■ AUTHOR INFORMATION

Corresponding Author

* Tel.: 1-541-737-6747. Fax: 1-541-737-2062. Email: Michael.Lerner@oregonstate.edu.

Notes

The authors declare no competing financial interest.

■ ACKNOWLEDGMENT

The authors acknowledge TGA and PXRD instrument support by Prof. Mas Subramanian (OSU Chemistry). Footprint area calculations were assisted by Zheng Wang (CAAM, Rice Univ.). Xiaochao Liu and Xin Li (OSU Chemistry) provided helpful suggestions.

■ REFERENCES

(1) Schöllhorn, R. Intercalation chemistry. *Physica B+C*. **1980**, *99*, 89-99.

(2) Selig, H.; Ebert, L. B. Graphite intercalation compounds. *Adv. Inorg. Chem. Radiochem.* **1980**, *23*, 281-327.

(3) Ouvrard, G.; Guyomard, D. Intercalation chemistry. *Curr. Opin. Solid State Mater. Sci.* **1996**, *1*, 260-267.

(4) Dresselhaus, M. S.; Dresselhaus, G. Intercalation compounds of graphite. *Adv. Phys.* **2002**, *51*, 1-186.

(5) Besenhard, J. O.; Möhwald, H.; Nickl, J. J. Electronic conductivity and structure of DMSO-solvated A^+- and $NR4^+$-graphite intercalation compounds. *Carbon*. **1980**, *18*, 399-405.

(6) Hérold, C.; Hérold, A.; Lagrange, P. New synthesis routes for donor-type graphite intercalation compounds. *J. Phys. Chem. Solids.* **1996**, *57*, 655-662.

(7) Toshiaki, E.; Masatsugu, S.; Morinobu, E. *Graphite Intercalation Compounds and Applications*. Oxford University Press: New York, USA, 2003.

(8) Sorokina, N.; Nikol'skaya, I.; Ionov, S.; Avdeev, V. Acceptor-type graphite intercalation compounds and new carbon materials based on them. *Russian Chem. Bull.* **2005**, *54*, 1749-1767.

(9) Jacobson, A. J.; Nazar, L. F. Intercalation Chemistry. *Encycl. Inorg. Bioinorg. Chem.* **2011**, 1-37.

(10) Matsumoto, K.; Takagi, K.; Hagiwara, R. Electrochemical synthesis of graphite-tetrafluoroaluminate intercalation compounds. *J. Electrochem. Soc.* **2012**, *159*, H876-H880.

(11) Safran, S. Stage ordering in intercalation compounds. *Solid State Phys.* **1987**, *40*, 183-246.

(12) Boehm, H. P.; Setton, R.; Stumpp, E. Nomenclature and terminology of graphite intercalation compounds (IUPAC Recommendations 1994). *Pure App. Chem.* **1994**, *66*, 1893-1901.

(13) Armand, M.; Touzain, P. Graphite intercalation compounds as cathode materials. *Mater. Sci. Eng.* **1977**, *31*, 319-329.

(14) Ohzuku, T.; Iwakoshi, Y.; Sawai, K. Formation of lithium-graphite intercalation compounds in nonaqueous electrolytes and their application as a negative electrode for a lithium ion (shuttlecock) cell. *J. Electrochem. Soc.* **1993**, *140*, 2490-2498.

(15) Wang, F.; Yi, J.; Wang, Y.; Wang, C.; Wang, J.; Xia, Y. Graphite intercalation compounds (GICs): A new type of promising anode material for lithium-ion batteries. Adv. Energy Mater. **2014**, *4*, 1300600.

(16) Purewal, J. J.; Keith, J. B.; Ahn, C. C.; Fultz, B.; Brown, C. M.; Tyagi, M. Adsorption and melting of hydrogen in potassium-intercalated graphite. *Phys. Rev. B*. **2009**, *79*, 054305.

(17) Skowroński, J. M.; Krawczyk, P. Improved hydrogen sorption/desorption capacity of exfoliated NiCl2-graphite intercalation compound effected by thermal treatment. *Solid State Ionics*. **2010**, *181*, 653-658.

(18) Tryba,B.; Przepiórski, J.; Morawski, A. W. Influence of chemically prepared H2SO4-graphite intercalation compound (GIC) precursor on parameters of exfoliated graphite (EG) for oil sorption from water. *Carbon*. **2003**, *41*, 2013-2016.

(19) Celzard, A.; Marêché, J. F.; Furdin, G. Modelling of exfoliated graphite. *Prog. Mater. Sci.* **2005**, *50*, 93-179.

(20) Kang, F.; Zheng, Y. –P.; Wang, H. –N.; Nishi, Y.; Inagaki, M. Effect of preparation conditions on the characteristics of exfoliated graphite. *Carbon*. **2002**, *40*, 1575-81.

(21) Wei, T.; Fan, Z.; Luo, G.; Zheng, C.; Xie, D. A rapid and efficient method to prepare exfoliated graphite by microwave irradiation. *Carbon*. **2009**, *47*, 337-339.

(22) Geng, Y.; Zheng, Q.; Kim, J. -K. Effects of stage, intercalant species and expansion technique on exfoliation of graphite intercalation compound into graphene sheets. *J. Nanosci. Nanotechnol.* **2011**, *11*, 1084-1091.

(23) Makotchenko, V. G.; Grayfer, E. D.; Nazarov, A. S.; Kim, S. J.; Fedorov, V. E. The synthesis and properties of highly exfoliated graphites from fluorinated graphite intercalation compounds. *Carbon*. **2011**, *49*, 3233-3241.

(24) Truong, Q. –T.; Pokharel, P.; Song, G. S.; Lee, D. -S. Preparation and characterization of graphene nanoplatelets from natural graphite via intercalation and exfoliation with tetraalkylammoniumbromide. *J. Nanosci. Nanotechnol.* **2012**, *12*, 4305-4308.

(25) Cooper, A. J.; Wilson, N. R.; Kinloch, I. A.; Dryfe, R. A. Single stage electrochemical exfoliation method for the production of few-layer graphene via intercalation of tetraalkylammonium cations. *Carbon*. **2014**, *66*, 340-350.

(26) MacFarlane, D.; Meakin, P.; Sun J.; Amini N.; Forsyth, M. Pyrrolidinium imides: a new family of molten salts and conductive plastic crystal phases. *J. Phys. Chem. B*. **1999**, *103*, 4164-4170.

(27) Zhou, Q.; Henderson, W. A.; Appetecchi, G. B.; Montanino, M.; Passerini, S. Physical and electrochemical properties of N-alkyl-N-methylpyrrolidinium bis(fluorosulfonyl)imide ionic liquids: $PY_{13}FSI$ and $PY_{14}FSI$. *J. Phys. Chem. B*. **2008**, *112*, 13577-13580.

(28) Hayyan, M.; Mjalli, F. S.; Hashim, M. A.; AlNashef, I. M.; Mei, T. X. Investigating the electrochemical windows of ionic liquids. *J. Ind. Eng. Chem*. **2013**, *19*, 106-112.

(29) Sirisaksoontorn, W.; Lerner, M. M. Preparation of a homologous series of tetraalkylammonium graphite intercalation compounds. *Inorg. Chem*. **2013**, *52*, 7139-7144.

(30) Sirisaksoontorn, W.; Lerner, M. M. The electrochemical synthesis of the graphite intercalation compounds containing tetra-n-alkylammonium cations. *ECS J. Solid State Sci. Technol.* **2013**, *2*, M28-M32.

(31) Ruch, P. W.; Hahn, M.; Rosciano, F.; Holzapfel, M.; Kaiser, H. Scheifele, W. *et al*. In situ X-ray diffraction of the intercalation of $(C_2H_5)_4N^+$ and BF_4^- into graphite from acetonitrile and propylene carbonate based supercapacitor electrolytes. *Electrochimica Acta*. **2007**, *53*, 1074-1082.

(32) Wang, H.; Yoshio, M. Feasibility of quaternary alkyl ammonium-intercalated graphite as negative electrode materials in electrochemical capacitors. *J. Power Sources.* **2012**, *200*, 108-112.

(33) Sirisaksoontorn, W.; Lerner, M. M. The effect of surface passivation on the preparation and stability of the graphite intercalation compounds containing tetra-n-alkylammonium cations. *Carbon*. **2014**, *69*, 582-587.

(34) Katayama, Y.; Morita, T.; Miura, T. Study on anode reactions of secondary lithium batteries in room-temperature ionic liquids. *Yoyuen oyobi Koon Kagaku*. **2006**, *49*, 82-86.

(35) Zheng, H.; Jiang, K.; Abe, T.; Ogumi, Z. Electrochemical intercalation of lithium into a natural graphite anode in quaternary ammonium-based ionic liquid electrolytes. *Carbon*. **2006**, *44*, 203-210.

(36) Tariq, M.; Podgoršek, A.; Ferguson, J.; Lopes, A.; Costa, G. M.; Pádua, A. *et al*. Characteristics of aggregation in aqueous solutions of dialkylpyrrolidinium bromides. *J. Colloid Interface Sci.* **2011**, *360*, 606-616.

(37) Zhang, L.; Zhang, H.; Luo, H.; Zhou, X.; Cheng, G. Novel chiral ionic liquid (CIL) assisted selectivity enhancement to (L)-proline catalyzed asymmetric aldol

reactions. *J. Brazilian Chem. Soc.* **2011**, *22*, 1736-1741.

(38) Maluangnont, T.; Lerner, M. M.; Gotoh, K. Synthesis of ternary and quaternary graphite intercalation compounds containing alkali metal cations and diamines. *Inorg. Chem.* **2011**, *50*, 11676-11682.

(39) Sirisaksoontorn, W.; Adenuga, A. A.; Remcho, V. T.; Lerner, M. M. Preparation and characterization of a tetrabutylammonium graphite intercalation compound. *J. Am. Chem. Soc*. **2011**, 133, 12436-12438.

(40) Zhang, X.; Lerner, M. M. Chemical synthesis of graphite perfluorooctanesulfonate using K_2MnF_6 in hydrofluoric acid or mixed acid solutions. *Chem. Mater.* **1999**, *11*, 1100-1109.

(41) Zhao, Y. H.; Abraham, M. H.; Zissimos, A. M. Fast calculation of van der Waals volume as a sum of atomic and bond contributions and its application to drug compounds. *J. Org. Chem.* **2003**, *68*, 7368-7373.

(42) Maluangnont, T.; Bui, G. T.; Huntington, B. A.; Lerner, M. M. Preparation of a homologous series of graphite alkylamine intercalation compounds including an unusual parallel bilayer intercalate arrangement. *Chem. Mater.* **2011**, *23*, 1091-1095.

(43) Umebayashi, Y.; Mitsugi, T.; Fujii, K.; Seki, S.; Chiba, K.; Yamamoto, H. *et al*. Raman spectroscopic study, DFT calculations and MD simulations on the conformational isomerism of N-alkyl-N-methylpyrrolidinium bis-(trifluoromethanesulfonyl) amide ionic liquids. *J. Phys. Chem. B*. **2009**, *113,* 4338-4346.

(44) Bottomley, M. J.; Parry, G. S.; Ubbelohde, A. R.; Young, D. A. 1083. Electrochemical preparation of salts from well-oriented graphite. *J. Chem. Soc.*, **1963**, 5674-5680.

(45) Besenhard, J.; Fritz, H. P. On the stage-wise oxidation of graphite in nonaqueous, neutral electrolytes. *Z. Naturforsch.* **1972**, 27b, 1294-1298.

(46) Placke, T.; Schmuelling, G.; Kloepsch, R.; Meister, P.; Fromm, O.; Hilbig, P.; Meyer, H. -W.; Winter, M. In situ X-ray Diffraction Studies of Cation and Anion Intercalation into Graphitic Carbons for Electrochemical Energy Storage Applications. *Z. Anorg. Allg. Chem.*, **2014**, *640*, 1996-2006.

Table of Contents (TOC) /Abstract Graphics